Environmental Science: Atmospheres

ROYAL SOCIETY OF CHEMISTRY

PAPER

View Article Online
View Journal | View Issue



Cite this: *Environ. Sci.: Atmos.*, 2023, **3**, 1791

# Atmospheric aging modifies the redox potential and toxicity of humic-like substances (HULIS) from biomass burning†

Chunlin Li, [ae] Diego Calderon-Arrieta, [b] Michal Pardo, [a] Dongmei Cai, [c] Alexander Laskin, [bd] Jianmin Chen [c] and Yinon Rudich [*a]

This study investigated the redox potential and toxicological changes of wood smoldering emitted HULIS due to reactions in the atmosphere and in neutral lung fluids. Fresh HULIS aerosols exhibited substantial oxidative potential (OP) and antioxidant capacity (AOC). Nighttime oxidation *via* heterogeneous $O_3$ or $NO_3^{\bullet}$ reactions impacted HULIS OP and AOC differently, with high humidity enhancing $O_3$ uptake and HULIS oxidation, causing a significant reduction in their redox potentials. The effective rate constants for HULIS redox-active components (RACs) by $O_3$ reaction increased with RH (<1.5% to 75%), with values of $(3.2–12.7)\times10^{-18}$ and $(1.8–9.7)\times10^{-18}$ $cm^3$ $mol^{-1}$ $s^{-1}$ for antioxidant moieties and oxidant components, respectively. The corresponding rate constants for $NO_3^{\bullet}$ reactions were $1.2 \times 10^{-14}$ and $3.9 \times 10^{-15}$ $cm^3$ $mol^{-1}$ $s^{-1}$. The endpoint cytotoxicity of HULIS, studied with lung epithelial cells, correlated well with the changes in OP, suggesting OP as a good indicator of HULIS oxidative toxicity. Redox reactions of fresh and atmospherically aged HULIS in neutral lung fluid mimics decreased their OP and AOC accompanied by $H_2O_2$ generation. The $H_2O_2$ yields were determined by both OP and AOC of HULIS, and the addition of lung fluid antioxidants amplified the $H_2O_2$ yield. Atmospheric aging retarded the decay of the redox potential and abated $H_2O_2$ yield, demonstrating that the remaining RACs in aged HULIS have relatively longer lifetimes against intrinsic reactions in the lung fluid environment. This study underscores the need to consider atmospheric transformations and lung fluid aqueous reactions when evaluating the health impact of HULIS and related organic aerosols.

Received 4th July 2023
Accepted 22nd October 2023

DOI: 10.1039/d3ea00104k

rsc.li/esatmospheres



## Environmental significance

Humic-like substances (HULIS) released from biomass burning account for a major portion of regional and global $PM_{2.5}$ pollution and cause a great threat to public health. We found that atmospheric transformation through $O_3$ or $NO_3^{\bullet}$ reaction at nighttime altered the redox potential and cytotoxicity of HULIS aerosols. Moreover, such modification by atmospheric chemistry determined the intrinsic redox-reactions and toxic results of inhaled HULIS aerosol in the lung fluids. The findings illustrated the dynamic health effect of HULIS, and highlight the importance of considering multiphase chemistry occurring in the atmosphere and in the respiratory system to assess the overall health effect of organic aerosols.

## 1. Introduction

Humic-like substances (HULIS) emitted by biomass burning are ubiquitous in the atmosphere and contribute significantly to the global organic aerosol mass. HULIS attract attention because of their great burden to climate and public health.[1,2] Worldwide climate warming and drying increase wildfire frequency and severity, leading to high regional loading of HULIS-containing smoke pollution originating from near and remote fires. Such high smoke episodes lead to deterioration of air quality and exposure to hazardous materials.[3] HULIS are well-known environmental hazardous materials containing carbonaceous chromophores and redox-active compounds (RACs) with low hygroscopicity and polarity, such as heterocyclic, phenolic, and quinoid compounds.[4–6] As HULIS is

[a]*Department of Earth and Planetary Sciences, Weizmann Institute of Science, 7600001, Israel. E-mail: yinon.rudich@weizmann.ac.il*
[b]*Department of Chemistry, Purdue University, West Lafayette 47907, USA*
[c]*Department of Environmental Science & Engineering, Fudan University, Shanghai, 236400, China*
[d]*Department of Earth, Atmosphere and Planetary Sciences, Purdue University, West Lafayette 47907, USA*
[e]*College of Environmental Science and Engineering, Tongji University, Shanghai 200072, China*

† Electronic supplementary information (ESI) available: Assisting details of chemical box modeling of atmospheric aging, acellular assays, elemental quantification, molecular analysis, and lifetime assessment of HULIS together with standard redox-active compounds test in lung fluid mimics are provided in ESI, including 8 texts, 16 figures, and 2 tables. See DOI: https://doi.org/10.1039/d3ea00104k

transported in the atmosphere, its chemical complexity and associated properties are further exacerbated.

The fate of organic aerosols in relation to climate and health effects depends on their atmospheric transformation and deposition within the human respiratory systems.[7] The atmospheric transformations primarily involve reactions with oxidants ($O_3$, $NO_3^{\bullet}$, $OH^{\bullet}$, *etc.*) and photochemistry by solar radiation, leading to multi-phase oxidation and decomposition of aerosol constituents.[8–11] Inhaled organic aerosols interact in the lung with the lining fluid through dissociation and redox reactions, causing adverse health effects, such as inflammation, oxidative impact, genotoxicity, and cell death.[12–16] Oxidative stress, one of the most prominent mechanisms, can be induced by the generation of cellular reactive oxygen species (ROS) and antioxidant consumption. Oxidative potential (OP) is often proposed as a promising alternative indicator of aerosol oxidative toxicity beyond the mass concentration.[17,18] HULIS in organic aerosols is a major OP contributor, which drives oxidative stress to the respiratory system upon inhalation.[19,20] Nevertheless, HULIS also possesses considerable antioxidant capacity (AOC) that can scavenge ROS radicals and potentially counteract oxidative damage to the human body.[21,22] It has been reported that the toxicity of humic substances in soils and waters depends on their redox potential.[23] The overall effect of HULIS on health can result from a fine balance between ROS production and antioxidant capacity.

Extensive research has been conducted to investigate the role of photochemistry in modifying the toxicity of secondary organic aerosols (SOA) from biomass burning, anthropogenic and biogenic emissions. The cytotoxicity of numerous SOA following photooxidation, the ROS speciation and yield from these SOA in simulated lung fluids and other liquids have been studied. The underlying mechanisms highly depend on the compositions and aging of SOA.[14,24–29] However, there is still ongoing discussion about the changes in SOA toxicity following the photooxidation.[30] Furthermore, while the importance of OP and oxidative stress has been emphasized, the AOC of SOA has been largely overlooked, potentially leading to a biased assessment of the overall adverse health effects of organic aerosols thus limiting the understanding of the associated mechanisms. The high reactivity of HULIS in multi-phase environmental chemistry has been highlighted.[1] Yet, the modification of HULIS intrinsic redox potential and cytotoxicity remain unclear. Additionally, the behavior of atmospherically processed HULIS in the lung fluid environment needs to be better understood.

Compared to photooxidation, the role of $O_3$ and $NO_3^{\bullet}$ reactions, which govern nighttime atmospheric chemistry, in mediating the toxicity of organic aerosol received less attention. Heterogeneous $O_3$ reactions are an important aging pathway of organic aerosols throughout day and night. Humidity is an important environmental parameter that influences $O_3$ oxidation by modifying aerosol phase, viscosity, diffusion, and the reactions.[31–35] However, the effect of humidity on the toxicity-related transformations of SOA has not been investigated thoroughly, and relevant studies yielded mixed results. It has been suggested that RH may influence the lifetime and degradation rates of the condensed-phase toxic compounds by mediating the aerosol phase state.[36–38] $NO_3^{\bullet}$, which forms from the reaction of $O_3$ and $NO_x$, is a more efficient oxidant than $O_3$ and denotes anthropogenic pollution in the air.[8,9] The nighttime aging pathway dominated by $NO_3^{\bullet}$ reactions is particularly relevant in biomass-burning plumes.[9,39] Despite the hypothesis that the aging of organic aerosols by $NO_3^{\bullet}$ may play a crucial role in their toxicity, limited studies have explored this topic.[25,40]

Inspired by the above knowledge gaps, we conducted laboratory experiments simulating the atmospheric heterogeneous agings of HULIS aerosols through nighttime oxidation by $NO_3^{\bullet}$ and $O_3$ under varying RH conditions. The resulting chemical transformations, the associated changes in particle acellular redox potentials (AOC and OP), and cytotoxicity were examined. The rate constants of HULIS-associated RACs for reactions with $O_3$ and $NO_3^{\bullet}$ were estimated. Moreover, the dynamic behaviors of atmospherically processed HULIS were explored in simulated lung fluids, both in the presence and absence of antioxidants, with respect to the intrinsic changes in the redox potential and the generation of ROS.

## 2. Experimental methods

### 2.1 HULIS preparation and simulating atmospheric heterogeneous aging

As described in previous studies,[4] wood smoldering emissions were collected to prepare HULIS samples. Briefly, the water-soluble fraction of the smoldering emissions was isolated *via* phase separation. After filtration through PTFE membrane syringes (0.2 μm porosity, Whatman), the clear water solution was acidified to pH 2.0 with HCl and subjected to solid phase-extraction (SPE) using a hydrophobic–lipophilic balance (HLB) SPE cartridge (3 mL, bed wt. 60 mg, Supelco®). The cartridge retains HULIS, while eluting inorganic salts and highly polar organic compounds. The relatively hydrophobic HULIS was eluted into methanol (>99.9%, Merck), evaporated to dryness, and stored at −20 °C for later use. In the experiments, the dried HULIS were redissolved into deionized water and nebulized to generate particles.

Heterogeneous oxidation of the dehydrated HULIS particles was performed utilizing a dark aerosol flow tube reactor (AFR) system, as schematically shown in Fig. S1A.† Specifically, three scenarios for nighttime aging of HULIS aerosols were simulated: (a) dry ozonolysis, (b) reaction with $NO_3^{\bullet}$, and (c) RH-dependent $O_3$ oxidation. The AFR maintained a total flow of 4.0 LPM, allowing for aerosol residence time of approximately 4.5 min. To initiate the oxidation reactions, ozone in a concentration range of 5–25 ppm was initially provided by an external ozone generator (Model 610, Jelight Inc.) and monitored using an ozone monitor (2B Technology, model 160L) at the AFR exit. RH in the range of 30–75% was controlled by adjusting the flow of humidified $N_2$ through a Nafion tube. $N_2O_5$ and $NO_3^{\bullet}$ for reactions with HULIS were produced by mixing NO with $O_3$ in a Teflon tube prior to entering the AFR. $O_3$ uptake coefficients by the HUILIS aerosol were determined under $NO_x$-free conditions and subsequently applied to estimate the $NO_3^{\bullet}$ sink to HULIS particles using a chemical box model.[41,42] To be noted, the study used high oxidant exposures to achieve equivalent oxidation results of aerosols over the course of long-term

 

transport in the atmosphere.[43,44] Detailed information regarding the experimental method and results can be found in the ESI† of Text S1 (Fig. S2, S3 and Table S1).

Following a series of denuders, the HULIS particles from the AFR were monitored online for concentration, bulk chemical composition, and optical properties. Meantime, HULIS particles were collected on Teflon filters (0.2 μm porosity, 47 mm diameter, Pall) for subsequent offline molecular analysis, toxicity assessment, and associated tests.

### 2.2 HULIS aerosol endpoint changes

**2.2.1 Measurements of optical properties.** The particle size and light wavelength-resolved extinction coefficients between 315 and 650 nm (resolution of 0.5 nm) were measured using a broadband cavity-enhanced spectroscopy (BBCES) system. The complex refractive index (RIs = $n$ + i$k$, real part of $n$ and imaginary part of $k$ correspond scattering and absorption) for HULIS aerosols were retrieved based on Mie theory. Detailed descriptions of the BBCES operation and Mie theory retrieval of RIs can be found elsewhere.[41,42]

**2.2.2 Chemical transformations.** Chemical changes of the bulk HULIS aerosols resulting from the AFR process were monitored in real-time using a high-resolution time-of-flight aerosol mass spectrometer (HR-Tof-AMS). Various parameters were derived from mass spectra collected in alternating W and V modes, including the elemental ratios (O/C, H/C, and N/C), the organic matter to organic carbon (OM/OC) ratio, categorized-fragment ($C_xH_y^+$, $C_xH_yO^+$, $C_xH_yO_z^+$, $C_xH_yO_iN_p^+$, and $NO_y^+$, $x$, $y$, $p \geq 1$, $z$, $i > 1$), and specific ions (such as $m/z$-43 $C_2H_3O^+$ and $m/z$-44 $CO_2^+$) fractions of HULIS.

In addition, HULIS samples collected on filters were extracted using acetonitrile for offline molecular analysis using an ultrahigh-performance liquid chromatography system (UHPLC, VanquishTM) coupled with a photodiode array detection (PDA) and a high-resolution orbitrap mass spectrometer Q Exactive™ (UHPLC-PDA-HRMS). Both positive and negative modes of electrospray ionization (ESI) sources were utilized owing to its high preference in detecting polar compounds.[45] HRMS data acquisition covered a mass range of $m/z$ 80–440. Details of the operation conditions and data analysis are provided in Text S2.† Double-bond equivalent (DBE), aromaticity index (AI), and maximum carbonyl ratio (MCR) values were calculated for the assigned neutral parent molecules.[46] These parameters provide insights into the chemical structure of HULIS and potential impacts on health.

**2.2.3 Redox potential changes.** As shown in Fig. S1B,† aerosolized HULIS collected on filters were first extracted into acetonitrile *via* vortex-shaking. The organic solutions passed through Teflon membrane filter syringes (0.2 μm porosity, Whatman) and were dried by a gentle flow of $N_2$. Then, the HULIS samples were reconstituted in a small amount of deionized water to create concentrated solutions of about 300 mg OC $L^{-1}$. The total organic carbon (TOC) content in the initial solution was quantified using a TOC analyzer (TOC-$V_{CPH}$, Shimadzu). Based on the TOC results, the initial solutions were diluted with deionized water, phosphate-buffered saline (PBS) solution, and surrogate lung fluid (SLF) at consistent HULIS concentration of 25 mg OC $L^{-1}$, which is relevant to environmental exposure and also provides a stock solution that keeps consistency among different experiments.[47] The PBS solution was treated with Chelex 100 sodium resin and had a pH of 7.4. The SLF solution was prepared with additional antioxidants (200 μM L-ascorbic acid sodium salt, 300 μM citric acid, 100 μM reduced L-glutathione, and 100 μM uric acid sodium salt) in the PBS solution.[48] The HULIS solutions were weakly acidic with pH ranging from 3.6 to 4.2 depending on the HULIS aging pathways.

The total peroxide content and redox potential of the HULIS diluted in water and PBS were immediately measured with a series of spectrophotometric assays. The total peroxide in equivalent of $H_2O_2$ ($H_2O_{2eq}$ in nmol μg $OC^{-1}$) was quantified using KI spectroscopic method.[49] In this study, the $H_2O_{2eq}$ represents the total ROS ($O_2^{\cdot-}$, OH$^\cdot$, $H_2O_2$) that can react with $I^-$ to produce $I_3^-$ with a characteristic absorbance at 350 nm.[50] The oxidative potential (OP) of HULIS was assessed in terms of the pseudo-first-order DTT depletion rate ($OP^{DTT}$, μM $min^{-1}$).[4,51] The $OP^{DTT}$ values were finally normalized to OC ($OP_{OC}^{DTT}$, pmol $min^{-1}$ μg $OC^{-1}$) or OM concentration ($OP_{OM}^{DTT}$, pmol $min^{-1}$ $\mu g^{-1}$). To ensure the reliability of the DTT assay, the $OP^{DTT}$ for standard 1,4-naphthaquinone and $H_2O_2$ as positive controls were frequently measured.

The total antioxidant capacity (AOC) of HULIS was quantified using the electron-transfer based ABTS method and Folin–Ciocalteu (FC) assay, yielding values in trolox and gallic acid equivalency (GAE).[52–54] Trolox is an analogue of Vitamin E, while gallic acid represents a group of polyphenols. To quantify the trolox equivalent antioxidant capacity (TEAC, nmol μg $OC^{-1}$), long-lived ABTS radical cation ($ABTS^{\cdot+}$) was generated through overnight reaction between 2.45 mM potassium persulfate (≥99%, Merck) and ABTS solution (2,2′-azino-di-(3-ethylbenzthiazoline sulfonic acid), A3219, Sigma-Aldrich). Before use, the light-blue $ABTS^{\cdot+}$ solution was diluted with deionized water to an absorbance of 0.700 ± 0.020 at 734 nm. The $ABTS^{\cdot+}$ scavenging ability by HULIS was determined by a decrease of absorption at 734 nm in comparison with a Trolox standard. For the quantification of gallic acid equivalency (GAE, nmol μg $OC^{-1}$), HULIS solutions were first mixed with FC reagent (F9252, Sigma Aldrich), then incubated at 37 °C for 30 min following the addition of 4.5 wt% $Na_2CO_3$ solution (>99%, Merck). The GAE of HULIS was extrapolated from the solution's specific absorbance at 750 nm using calibration curves of gallic acid. The redox potential (OP and AOC) measured in water and PBS was denoted by the corresponding subscript "w" and "PBS", such as $OP_{OC\_w}^{DTT}$ and $OP_{OC\_PBS}^{DTT}$. Detailed description of the redox potential quantification can be found in Text S3 and S4,† and the spectrophotometric calibration curves of standards are given in Fig. S4–S6.†

**2.2.4 Cytotoxicity.** Alveolar epithelial cells (A549, CCL-185, ATCC) were used to evaluate the cytotoxic changes of HULIS following heterogeneous aging. Fresh and three types of aged HULIS, namely, those oxidized under dry conditions and 45% RH by 25 ppm $O_3$, and after reacting with $NO_3^\cdot$, were reconstituted in deionized water at concentrations of 200 and 300 mg OC $L^{-1}$. A549 cells were exposed to these samples for 5 h, then cell

viability, cellular ROS generation, and lipid peroxidation were evaluated then, providing insights into the toxic effects of HULIS and the underlying mechanisms.[15] The results are expressed as the means ± standard deviation (SD) of at least two experiments. Detailed description for the cell culture, exposures, cellular assays, and statistical analysis of the results are found in Text S5.† The concentrations of the HULIS samples were determined in preliminary tests to be within detection range limits for the assays and also in consideration of acute respiratory exposure under severe smoke pollution events next to the fire sources.[16,55] It is noted that realistic exposure scenarios vary substantially, the estimated concentration of $PM_{2.5}$ that can deposit in the respiratory tract lining fluids can differ from several μg $L^{-1}$ to hundreds mg $L^{-1}$.[56] This study focuses mainly on toxicological changes of HULIS during nighttime atmospheric aging.

### 2.3 Evolution of HULIS aerosol in lung fluid mimics

To gain insight into the behavior of HULIS aerosols within the respiratory system following atmospheric transformation, 25 mg OC $L^{-1}$ of fresh and aged HULIS in PBS and SLF were incubated at 37 °C in the dark for 4 hours to mimic lung fluid condition. Throughout the experiment, we assumed a constant TOC concentration of HULIS. During the incubation period, we monitored the redox potential (OP and AOC) of HULIS in the PBS solutions and the production of $H_2O_{2eq}$ in both PBS and SLF solutions at hourly intervals. It is important to note that the evolution of redox potential and ROS generation only reflected the intrinsic behavior of HULIS in a simplified neutral lung fluid environment.

The operational blank and background signals were subtracted in all the measurements. Totally three batches of HULIS were prepared, and each batch was used for heterogeneous aging experiment incorporating with aerosol online characterization and offline analysis. Each filter sample was characterized in duplicate of redox potential. Molecular composition, cytotoxicity, and lung fluid evolution of the fresh and aged HULIS were tested for at least two times. Only average results are discussed in this study. All chemical reagents used were of the highest available purity, and assay solutions were freshly prepared daily during the experiments.

## 3. Results and discussions

### 3.1 Chemical changes in HULIS after atmospheric aging

Fig. 1 shows the comprehensive chemical transformations of HULIS aerosols resulting from reactions with varying $O_3$ or $NO_3^{\bullet}$. The changes in elemental composition are summarized in Table S2.† Fig. 1A and D demonstrate that increasingly dry $O_3$ exposure led to the gradual oxidation of HULIS. Functionalization and peroxide/alcohol/carboxyl generation are suggested based on the flat Van Krevelen (VK) slope and the increased intensity of carboxyl fragments (*f*44). Fig. 1B and E show significant $O_3$ oxidation of HULIS with increasing RH, resulting in extensive oxygenation, hydrogen abstraction, and production of carboxyl and carbonyl compounds. These transformations shift HULIS from less-oxidized (LO-OOA) to more-oxidized oxygenated organic aerosols (MO-OOA). From the $O_3$ surface uptake analysis of HULIS particles (Text S1, Fig. S2†), increasing RH from 30% to 75% accelerated the $O_3$ effective uptake coefficient by a factor of 2–3. Moreover, the particulate elemental mass changes (Text S6, Fig. S7†) indicated a significant loss of carbon and nitrogen and increased oxygen content in HULIS particles following RH-dependent $O_3$ oxidation, particularly at RH above 45%. These results are in line with previous findings that humidity increases the surface uptake of $O_3$ by HULIS and modifies their chemical reactivity and reaction pathways, which in turn promotes oxidation followed by functionalization and fragmentation.[57] The effects of aging on HULIS likely follow the known $O_3$ reaction mechanisms involving unsaturated carbon double bond ozonolysis and cleavage that generate particulate carbonyl and carboxyl functionalities and volatile species.[58] The changes in the imaginary part of the refractive indices (RI) indicate that $O_3$ oxidation decomposed chromophores in HULIS (Fig. S8A†), thus reducing their light absorption. The rate of bleaching by ozonolysis also exhibited RH dependence.

In Fig. 1C and F, approximately 5- and 20 hours equivalent nocturnal exposure to ambient 20 ppt $NO_3^{\bullet}$ (Text S1†) induced similar evolution in the elemental ratios and *f*43 *vs.* *f*44 to that of $O_3$ oxidation. Still, it generated more nitrogen-containing ($C_xH_yO_iN_p^+$) and nitrate ($NO_y^+$) fragments in the HULIS aerosols (Fig. 1G). The higher characteristic fragment ratio of $NO^+/NO_2^+$ compared to that of ammonium nitrate (4.6 *vs.* 2.1) indicates organic nitrate or/and nitro-component formation. Extensive $NO_3^{\bullet}$ aging increased particulate $C_xH_yO_iN_p^+$ and $NO_y^+$ fragments from 4.0 wt% and 0.2 wt% to 7.7 wt% and 2.8 wt%, correspondingly. Numerous studies have reported the formation of nitrophenols and organonitrates together with other carbonyl and carboxyl functions following the rection of $NO_3^{\bullet}$ with biomass burning aerosols at night.[9,42] The enhanced light absorption (Fig. S8B†) following $NO_3^{\bullet}$ aging suggests the formation of secondary chromophores (probably nitroaromatics). In addition, minor fragmentation also occurred after maximal $NO_3^{\bullet}$ exposure, reflecting carbon loss (Fig. S7†).

The molecular composition of HULIS was studied using UHPLC-PDA-HRMS platform, which allowed the assessment of structural characteristics of individual components, such as Aromaticity Indices (AI), Maximum Carbonyl Ratios (MCR), and oxidation degrees. The assigned formulae of HULIS components were categorized based on these characteristics. Fig. 2A and S9A† of MCR-Van Krevelen diagram illustrate the high extent of aromaticity and unsaturation in fresh HULIS, indicating their susceptibility to oxidation by atmospheric oxidants. As shown in Fig. 2B–D, both $O_3$ and $NO_3^{\bullet}$ exposure induced the decomposition of HULIS and reshaped the distribution of their chemical structural composition, aromaticity, and unsaturation degree. $O_3$ oxidation, particularly at 45% RH, modified HULIS substantially, decreasing their ensemble molecular weight and leading to a higher contribution of more oxidized components with lower unsaturation degree and aromaticity. These findings suggest that aged HULIS likely possess lower toxicity and weaker light absorption properties. Reaction with high levels of $NO_3^{\bullet}$ produced oxidized compounds and reduced the unsaturation degree of HULIS components. Compared to dry

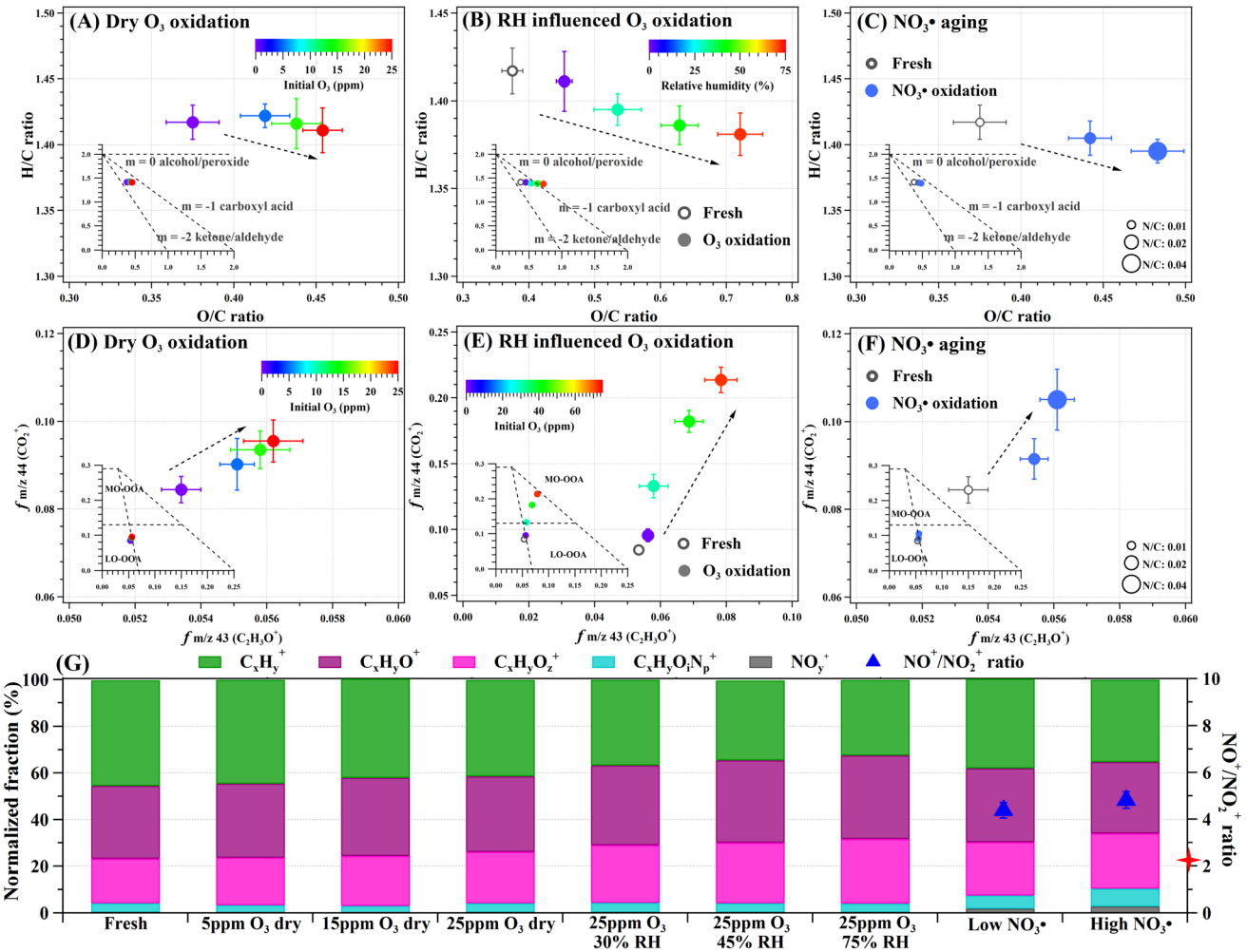


Fig. 1 HR-Tof-AMS measured chemical transformations of HULIS aerosols following dry ozonolysis (A and D), RH-dependent $O_3$ oxidation (B and E) and $NO_3^{\bullet}$-dominated heterogeneous aging (C and F). The plots show Van Krevelen (VK) diagrams, organic elemental ratios (A–C), and triangle plots of *f*43 *vs.* *f*44 (D–F). Panel G shows the ensemble-normalized fragments' compositions. A V–K plot is inserted in panel A–F. The dashed triangle zone in panel D–F constrains ambient oxygenated organic aerosol (OOA), two specific regions classify the oxidation level of OOA (less- and more-oxidized OOA, LO-OOA *vs.* MO-OOA). In panels A-F, the dashed arrows indicate the chemical trends with increasing $O_3$, RH and $NO_3^{\bullet}$. $NO^+/NO_2^+$ ratios in $NO_3^{\bullet}$ oxidized HULIS were specifically displayed as solid blue triangle in panel G. The red star at the right-hand *Y*-axis indicates $NO^+/NO_2^+$ ratio of 2.1 for $NH_4NO_3$ aerosols measured by the AMS.

ozonolysis, $NO_3^{\bullet}$ aging resulted in a more significant decrease in HULIS constituents with higher AI (>0.7), which can be attributed to the preferential reactions of aromatics and poly-aromatics with $NO_3^{\bullet}$. The heterogeneous aging reactions involving dry $O_3$ and $NO_3^{\bullet}$ resulted in relatively small overall chemical bulk changes, suggesting that only surface reactions occurred in dry HULIS particles. However, at 45% RH, $O_3$ uptake on the particle surface was facilitated, possibly due to faster diffusion and the reaction of $O_3$ within the aerosol, leading to more pronounced chemical transformations.

### 3.2 HULIS redox potential changes during atmospheric aging

The redox potential as a function of the oxidant normalized surface uptake by HULIS particles are shown in Fig. 3. The oxidant normalized surface uptake is defined as the total oxidant uptake divided by the particle surface area concentration and is related to the oxidation degree of HULIS. The specific values can be found in Table S2.† Fresh HULIS had $OP^{DTT}_{OC\_PBS}$ of 115.2 ± 8.6 pmol $min^{-1}$ μg $OC^{-1}$, with an equivalent 1,4-naphthoquinone content of 2.2 wt%. These values fall within the range of previously reported observations.[4,51,59] Notably, the $GAE_{\_PBS}$ of 4.8 nmol μg $OC^{-1}$ contributes to >40 wt% of fresh HULIS, demonstrating its high phenolic content.[21] The $TEAC_{\_PBS}$ of 5.6 nmol μg $OC^{-1}$ provides further evidence of the substantial antioxidant capacity of fresh HULIS. Intriguingly, our data reveal a strong correlation between GAE and TEAC (Fig. S10†), suggesting that phenolic electron-donating moieties act as the primary antioxidants throughout the aging process of HULIS.

Ozonolysis under dry conditions progressively reduced the HULIS AOC, with significant reduction in OP observed at $O_3$ beyond 15 ppm. The most extensive dry ozonolysis resulted in a 12% reduction in HULIS OP and a 20% decrease in AOC.

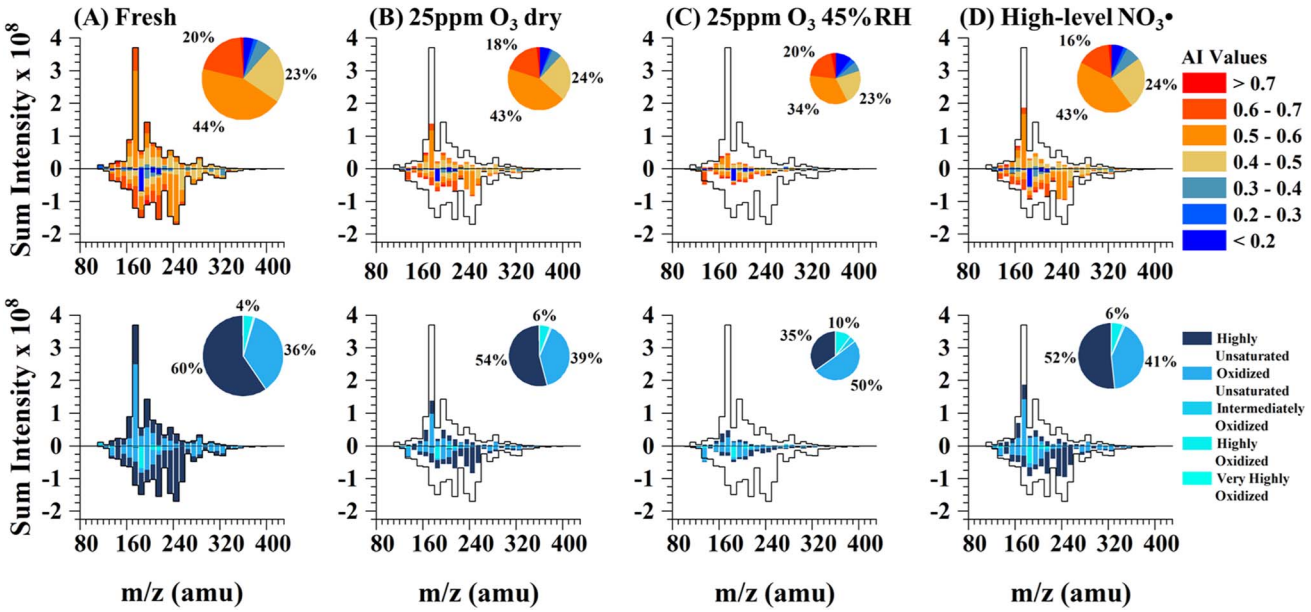


Fig. 2 UHPLC-PDA-ESI-HRMS measured molecular compositions and chemical features of CHO species in fresh (A) and heterogeneously aged (B–D) HULIS. In each panel, the positive and negative intensity corresponds to results detected from +ESI and −ESI mode, respectively. The histograms of molecular-weight distributions are compared with fresh HULIS. The assigned formulae are classified based on their aromaticity index value (upper panels) and structural oxidation degree (lower panels). The intensity-weighted fractions of each category are displayed by pie charts. The size of the pie chart reflects the abundance of the total assigned CHO molecules.

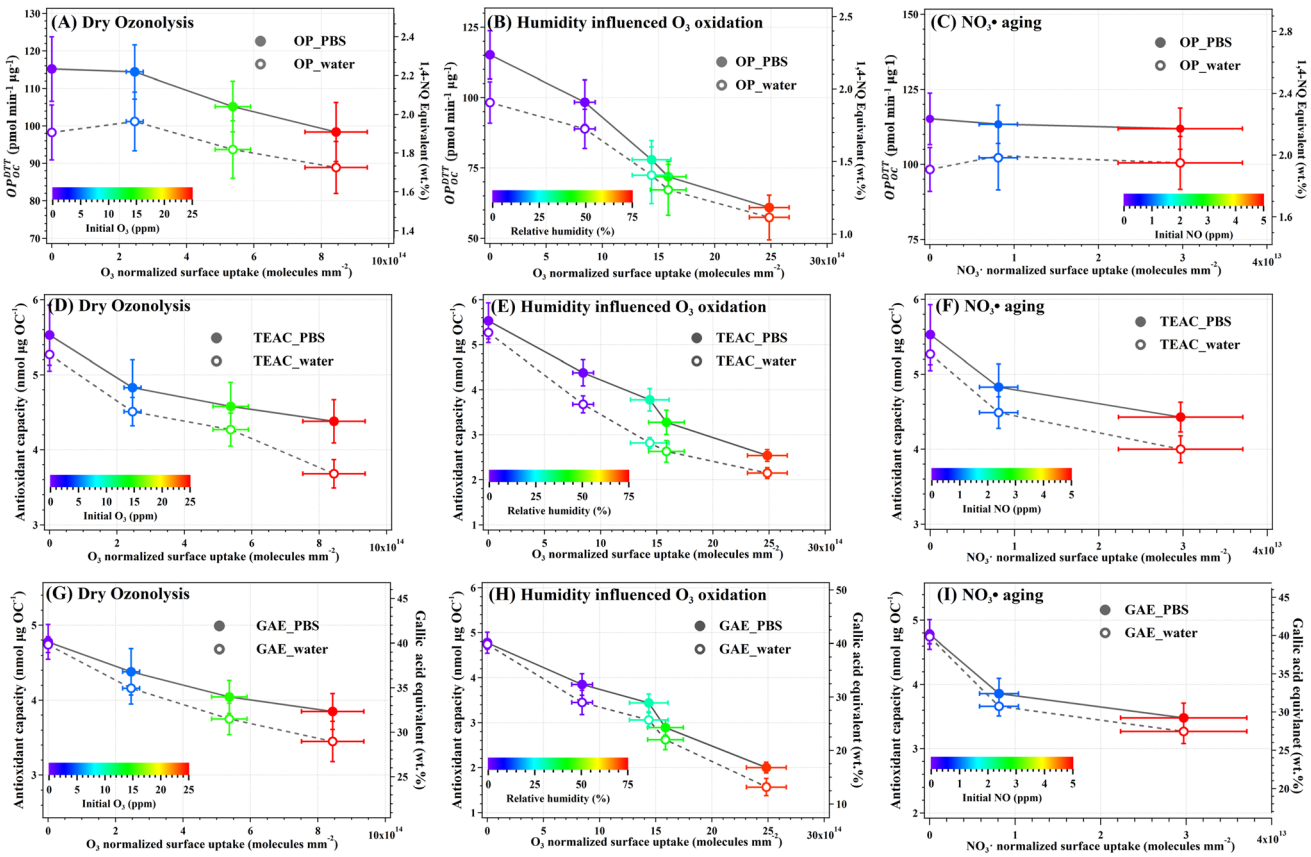


Fig. 3 Evolution of HULIS oxidative potential (A–C) and antioxidant capacity in terms of TEAC (D–F) and GAE (G–I) as a function of oxidant normalized surface uptake following heterogeneous agings, including dry ozonolysis at varying $O_3$ concentrations (A and D), RH-dependent $O_3$ oxidation (B and E), and $NO_3^{\bullet}$-dominated reactions (C and F). Redox potentials were compared for HULIS dissolved in deionized water and PBS (pH 7.4). The equivalent 1,4-naphthaquinone and gallic acid contents were calculated based on the HULIS OP and GAE results (right axil of panel A–C and G–I).

Ozonolysis under elevated humidity levels (≥30% RH) decreased HULIS OP and AOC, suggesting that increased RH enhances $O_3$ oxidation in parallel to the decomposition or deactivation of the redox-active components (RACs) within HULIS. Previous studies have investigated the decomposition of polyphenols and polyhydroxylated quinones through $O_3$ exposure at the air–water interface. The $O_3$ attack resulted in cleavage reactions and the generation of oxygenated low molecular weight species.[60] In line with our findings, $O_3$ oxidation and fragmentation of HULIS decreased their redox potential. The AMS results also indicated considerable carboxyl functionalization of HULIS during $O_3$ oxidation under humid conditions. The carboxyl group acts as an electron-accepting group and can decrease the antioxidant capacity of phenols by withdrawing electron density from the phenol ring.[21] This observation may also explain the observed decrease in HULIS AOC.

$NO_3^{\bullet}$ aging had a negligible effect on HULIS $OP_{OC}^{DTT}$, but it significantly decreased the $OP_{OM}^{DTT}$ (Table S2†). Additionally, $NO_3^{\bullet}$ reactions decreased the HULIS AOC, possibly due to the formation of nitroaromatics. The nitro group is a strong electron-withdrawing functionality, which can reduce the AOC of phenols and interfere with electron transfer in oxidant compounds, thereby decreasing their OP as well.[21]

In summary, the nighttime processes of heterogenous aging by $O_3$ or $NO_3^{\bullet}$ reduced HULIS AOC while exhibiting complex effects on their OP. Although the redox potentials of HULIS in PBS (pH ∼ 7.4) and water (pH < 4.2) showed a strong correlation, they generally displayed higher values in neutral solutions. These findings agree with previous studies in which solution pH enhanced both the OP and the electron-donating capacity (EDC) of humic substances by modifying their chemical structures and associated redox reactions.[4,22,61] Moreover, the phenolic carboxyl groups commonly dissociate at pH above 5. Unlike carboxyl groups (COOH), carboxylate ions ($COO^-$) do not possess electron-withdrawing properties. Therefore, the deprotonation of carboxylic groups enhances the AOC of phenols.[21] These factors may account for the significant differences between $TEAC_{\_PBS}$ and TEAC_w, particularly for HULIS that reacted with ozone to gain more carboxyl as indicated by the higher *f*44 (Fig. 1E), attributed to the formation of carboxyl-phenolic moieties in aged HULIS.

Nighttime atmospheric aging changed the mass and redox potential of HULIS. We therefore calculated the effective second-order kinetics for the depletion of redox-active moieties in HULIS aerosols due to reactions with $O_3$ or $NO_3^{\bullet}$. The rate constants are summarized in Table 1, the detailed calculations can be found in Text S7 (Fig. S11†). The depletion rate constants for both antioxidant moieties (*e.g.*, phenols) and oxidizing components (*e.g.*, quinones) in HULIS due to $O_3$ oxidation were similar and increased with RH, suggesting that RH not only promoted particle surface uptake of $O_3$ but also accelerated the relevant reaction rates. The calculated effective kinetics for the antioxidant moieties, represented by both GAE and TEAC, ranged from $3.2 \times 10^{-18}$ to $1.3 \times 10^{-17}$ $cm^3$ $mol^{-1}$ $s^{-1}$. These values are comparable with those reported phenol reaction kinetics of $(9.6–63.0) \times 10^{-18}$ $cm^3$ $mol^{-1}$ $s^{-1}$.[60,62,63] However, the average depletion rate with respect to $NO_3^{\bullet}$ reaction was $1.2 \times 10^{-14}$ $cm^3$ $mol^{-1}$ $s^{-1}$, which is 2–3 orders of magnitude lower than the relevant kinetics of phenols.[62,63] The apparent depletion rate is expected to be lower than those reported for intrinsic first-step reaction kinetics. Besides, the generated nitrophenols from $NO_3^{\bullet}$ reactions are polyphenols that interfere with the FC and ABTS assays (Fig. S13†). Both $O_3$ and $NO_3^{\bullet}$ oxidation resulted in the decomposition or deactivation of particulate oxidizing components that contribute to $OP_{OC\_PBS}^{DTT}$ of HULIS. The rate constant for the $O_3$ reaction increased from $1.8 \times 10^{-18}$ to $9.7 \times 10^{-18}$ $cm^3$ $mol^{-1}$ $s^{-1}$ as RH increased from <1.5% to 75%. The rate constant for $NO_3^{\bullet}$ reaction was $3.9 \times 10^{-15}$ $cm^3$ $mol^{-1}$ $s^{-1}$.

Using these kinetic values, we tentatively estimated the lifetime of HULIS RACs during nighttime atmospheric aging with respect to varying $O_3$ or $NO_3^{\bullet}$ concentrations (Text S7, Fig. S12†). Assuming a daily average $O_3$ concentration of 35 ppb, the half-lifetime of HULIS antioxidants against dry ozonolysis is about 66 hours. However, humidity accelerates the $O_3$ oxidation, shortening the lifetime of HULIS antioxidants to less than 19 hours at 75% RH. The corresponding half-lifetime of oxidizing components in HULIS decrease from approximate 123 to 23 hours. When aged with 20 ppt $NO_3^{\bullet}$, the half-lifetimes of antioxidants and oxidizing compositions were estimated to be about 33 and 100 hours, respectively. These results suggest that HULIS can have a profound impact on health during their long-range transport at night, emphasizing the role of RH in mediating the range of HULIS influence.

### 3.3 Changes of HULIS cytotoxicity during atmospheric aging

Fig. 4 shows significant cytotoxic effects on lung epithelial cells (A549) after 5 hours of exposure to fresh and atmospherically

Table 1 Effective second-order depletion rate constants in reaction with $O_3$ or $NO_3^{\bullet}$ for redox-active compounds that contribute to antioxidant capacity and oxidative potential of HULIS (1 atm, 295 k)

| Experiment condition | $K_{GAE\_PBS}$ ($cm^3$ $mol^{-1}$ $s^{-1}$) | $K_{TEAC\_PBS}$ ($cm^3$ $mol^{-1}$ $s^{-1}$) | $K_{OPOC\_PBS}^{DTT}$ ($cm^3$ $mol^{-1}$ $s^{-1}$) |
|---|---|---|---|
| Dry ozonolysis | $(3.24 \pm 0.37) \times 10^{-18}$ | $(3.57 \pm 0.71) \times 10^{-18}$ | $(1.82 \pm 0.55) \times 10^{-18}$ |
| 30%RH $O_3$ oxidation | $(4.12 \pm 0.93) \times 10^{-18}$ | $(4.70 \pm 0.98) \times 10^{-18}$ | $(4.84 \pm 1.09) \times 10^{-18}$ |
| 45%RH $O_3$ oxidation | $(7.23 \pm 1.49) \times 10^{-18}$ | $(7.48 \pm 1.47) \times 10^{-18}$ | $(6.82 \pm 1.50) \times 10^{-18}$ |
| 75%RH $O_3$ oxidation | $(1.27 \pm 0.24) \times 10^{-17}$ | $(1.15 \pm 0.21) \times 10^{-17}$ | $(9.69 \pm 1.96) \times 10^{-18}$ |
| RH-dependent $O_3$ oxidation[a] | $(2.36 + 0.80 \times e^{-RH/27.93}) \times 10^{-18}$ | $(1.89 + 1.55 \times e^{-RH/38.99}) \times 10^{-18}$ | $(1.64 + 0.11 \times RH) \times 10^{-18}$ |
| $NO_3^{\bullet}$ aging | $(1.35 \pm 0.51) \times 10^{-14}$ | $(1.06 \pm 0.37) \times 10^{-14}$ | $(3.92 \pm 1.18) \times 10^{-15}$ |

[a] Indicates the best exponentially and linearly regressed functions of RH-determined $O_3$ reaction kinetics. RH in unit of %. The redox potential results measured in PBS were applied.

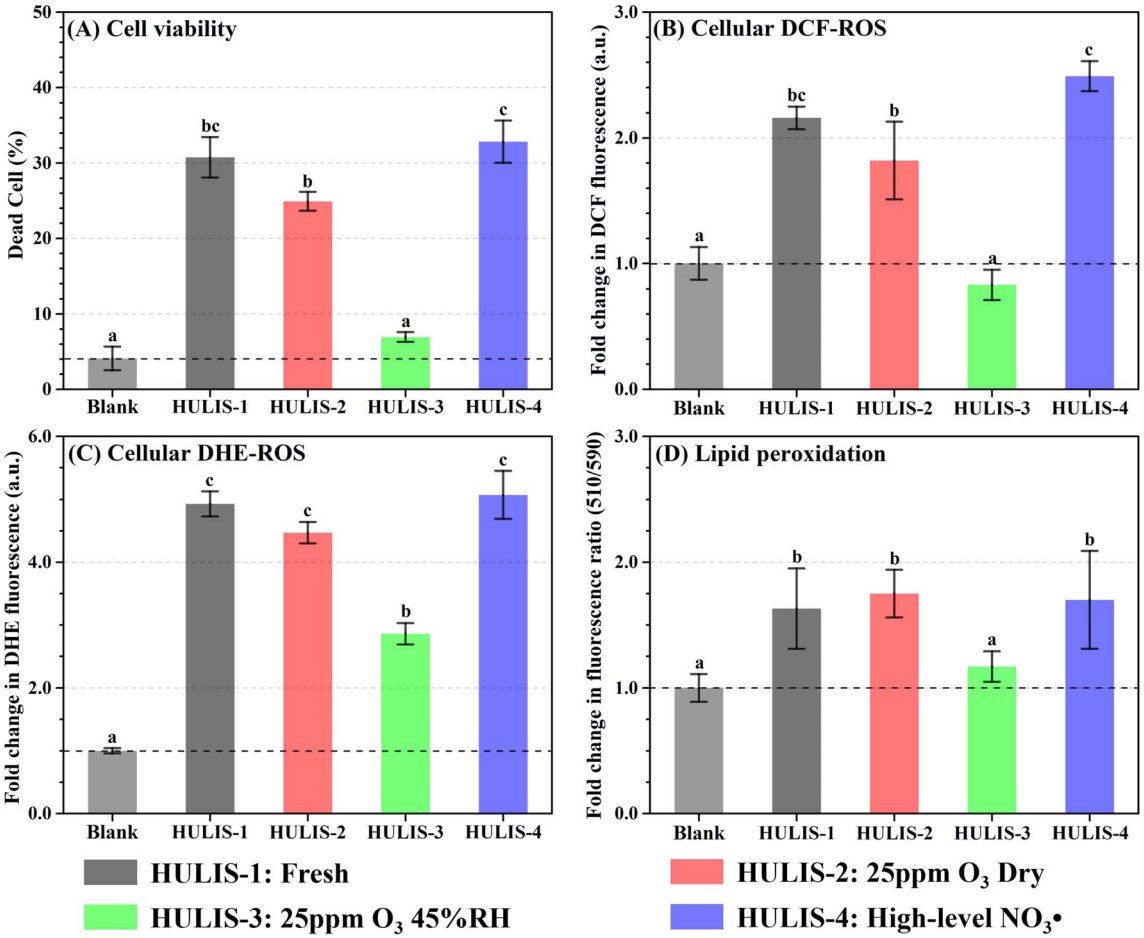


Fig. 4 Cytotoxicity of HULIS aerosols after atmospheric aging. (A) Cell viability after 5 hours' exposure with HULIS of 200 mg OC $L^{-1}$. Cellular ROS levels measured using dichlorodihydrofluorescein (DCF) (B) and dihydroethidium (DHE) (C) probes, respectively. (D) Lipid peroxidation measured using boron-dipyrromethene (BODIPY) fluorescent probes. Bar height and error bars represent arithmetic mean ± SEM of cell death and fluorescence normalized to operational blanks (controls, a.u.: arbitrary units), respectively. Mean with different letters are significant different at $p < 0.05$ (Turkey HSD test). The black dashed line clarifies the signal changes compared to blank. Fresh HULIS (HULIS-1) and three kinds of atmospheric processed HULIS were tested, including 25 ppm $O_3$ oxidized samples under dry (HULIS-2) and 45%RH (HULIS-3) conditions, and maximum $NO_3^{\bullet}$ oxidized samples (HULIS-4).

aged HULIS. As shown in Fig. 4A, more than 30% cell death was measured when exposed with 200 mg OC $L^{-1}$ of fresh HULIS compared to the blank treated cells. Exposure of the dry ozonolyzed HULIS also induced higher cell death than the blank, like the effect of fresh HULIS. In contrast, after oxidized by $O_3$ at 45% RH, the reacted HULIS had a similar effect as the blank with minimal cell death. Exposure of the $NO_3^{\bullet}$ reacted HULIS led to the highest cell death. The cell death trends were similar to the cellular generation of total ROS and $O_2^{\bullet-}$ and with lipid peroxidation extent (Fig. 4B–D). Moreover, both cell death and ROS generation reacted in a dose-dependent manner (Fig. S14†). The correlations between cellular ROS yields, lipid peroxidation, and cell death suggest that oxidative stress is a primary toxicological mechanism resulting from HULIS exposure.

The cytotoxicity of fresh and aged HULIS followed the OP pattern, suggesting that OP is a plausible metric for assessing HULIS toxicity.[18] Specifically, dry ozonolysis had a negligible effect on the cytotoxicity of HULIS towards A549 cells, with low cell death rate, total ROS levels, and $O_2^{\bullet-}$ generation. $O_3$ oxidation of HULIS under 45% RH decreased the redox potential and the cytotoxicity, making it almost non-toxic compared to the fresh HULIS. In contrast, $NO_3^{\bullet}$ aging had a positive effect on HULIS cytotoxicity, causing increased cell death, elevated levels of total ROS, and $O_2^{\bullet-}$ generation.

### 3.4 Evolution of HULIS redox potential and ROS generation in lung liquid environment

Inhaled nanoparticles can remain in the alveoli for up to 24 hours.[64] Previous relevant studies allowed 3–4 hours for redox reactions of organic aerosols in lung fluid environment to achieve equilibrium of ROS generation.[4,28] Therefore, we studied the toxicity of HULIS in neutral lung fluid mimics for 4 hours to investigate the dynamic evolution of deposited HULIS in the respiratory system. The results presented in Fig. 5A, B and S15A–F† indicate that under neutral conditions, both the OP and AOC of HULIS generally decreased, except for the fresh

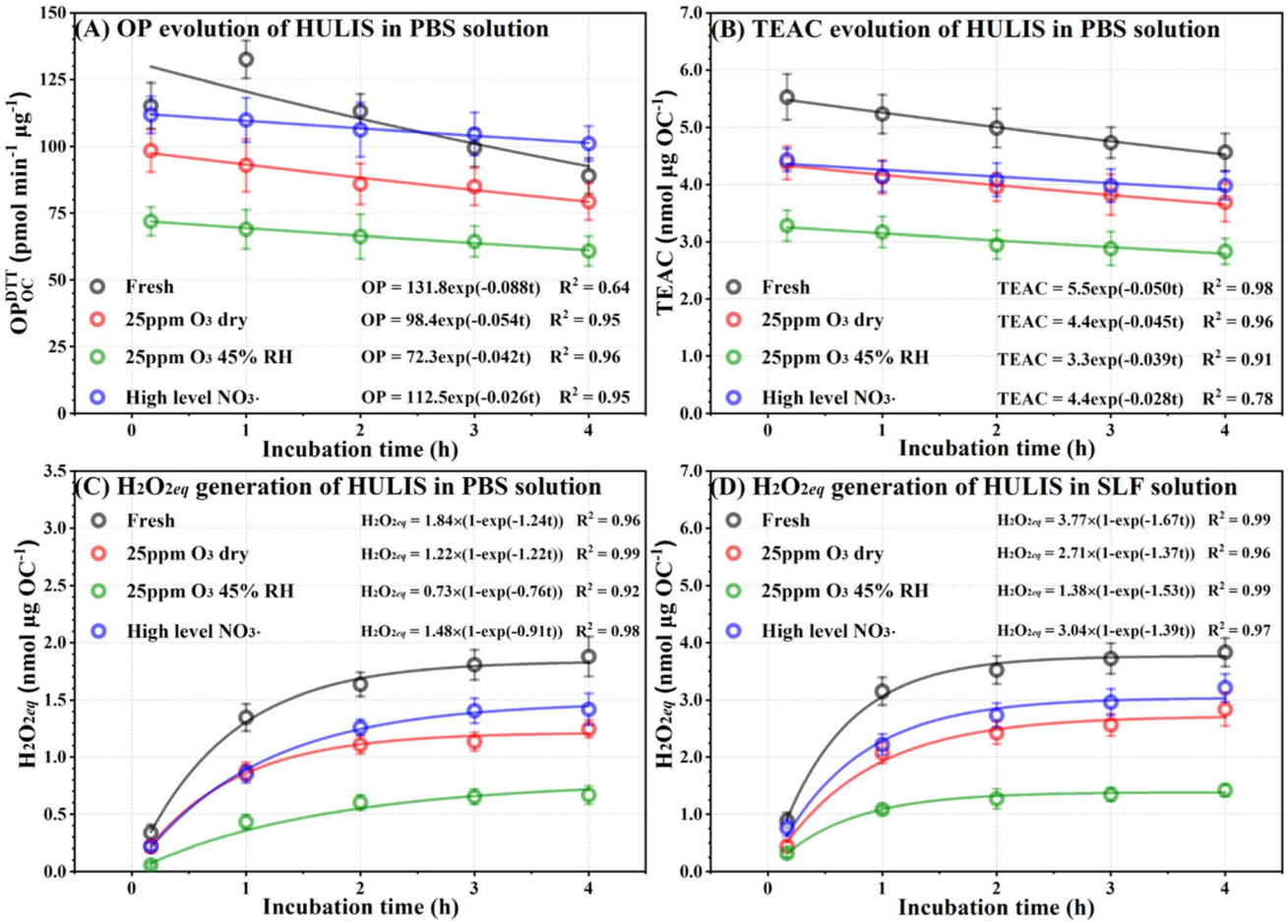


Fig. 5 Evolution of (A) OP, (B) TEAC, and (C) $H_2O_{2eq}$ generation for fresh and atmospherically aged HULIS in PBS solutions during a 4 h oxic incubation at 37 °C in the dark. (D) Parallel tests of $H_2O_{2eq}$ generation for HULIS in surrogate lung fluid (SLF). Results for 25 ppm $O_3$ oxidized and maximum $NO_3^{\bullet}$ aged HULIS are shown. The results of additional tests are given in Fig. S15.† The redox potentials and $H_2O_{2eq}$ were exponentially regressed using the Exp2PMod1 and BoxLucas1 functions, respectively, using OriginPro 2021.

samples, which showed an initial increase in OP before decreasing after 1 hour. This change in OP for fresh HULIS is consistent with previous findings suggesting a pH-promoted conversion mechanism of quinones through the autoxidation of hydroquinones and polyphenols.[4,65]

The redox potential followed an exponential decay, indicating an apparent first-order depletion or deactivation kinetics of both oxidizing and antioxidant moieties in all HULIS samples. Our study derived first-order depletion rate constants and we found that nighttime heterogeneous aging slowed down the reduction of HULIS redox potentials in PBS, demonstrating potentially weaker reactivity of the lowered RACs in atmospherically aged HULIS. Generally, the OP decreased more rapidly than the AOC, and the polyphenol contents declined at slower rates than the TEAC. For example, the fresh HULIS had pseudo-first-order decline rates of 0.088, 0.050, and 0.034 $h^{-1}$ for $OP_{OC\_PBS}^{DTT}$, TEAC and GAE, respectively. These rates decreased with HULIS oxidation by $O_3$ or $NO_3^{\bullet}$. The most oxidized HULIS (high $O_3$ exposure at 75% RH) displayed corresponding rates of 0.032, 0.037, and 0.012 $h^{-1}$, respectively. Maximum $NO_3^{\bullet}$ aging decreased these rates to 0.026, 0.028, and 0.008 $h^{-1}$, respectively. These results suggest that the RACs in atmospherically aged HULIS are more resilient toward intrinsic chemical reactions. On average, the OP and AOC of HULIS decreased by 16% and 11%, respectively, over a 4 hours period in a neutral lung fluid environment. Therefore, we opine that the intrinsic chemical reactions of HULIS in the lung fluid are not an important pathway in deactivating HULIS toxicants upon inhalation.

Fig. 5C, S15G and H† illustrate a rapid generation of $H_2O_{2eq}$ in all HULIS samples incubated in PBS, reaching a plateau within 3 hours. The temporal evolution of $H_2O_{2eq}$ followed Boxlucas growth model. Because fresh and atmospherically aged HULIS do not contain organoperoxides, the $H_2O_{2eq}$ cannot form from organoperoxide decomposition. The correlation between redox potential change and $H_2O_{2eq}$ generation, as well as the strong correlations between $H_2O_{2eq}$ yields and initial OP and AOC values, suggest that $H_2O_{2eq}$ is produced through redox reactions involving both antioxidant and oxidizing moieties within HULIS. To test this hypothesis, we used 1,4-napthaquinone and gallic acid as redox proxies. They were incubated individually or in combination in PBS (Text S8†). The functional

behavior of HULIS was only replicated when a mixture of 1,4-napthaquinone and gallic acid was used (see Fig. S16†), although the rates of redox potential changes differed, likely due to the greater complexity of the HULIS chemical compositions.

Additional antioxidants in the SLF increased the $H_2O_{2eq}$ generation in all HULIS samples, resulting in an approximately twofold increase in the final $H_2O_{2eq}$ yield (Fig. 5D, S15I and J†), suggesting that antioxidants contribute to the generation of $H_2O_{2eq}$. Tong *et al.* also found significantly higher ROS yields, particularly $H_2O_2$ and $O_2^{\cdot-}$, for naphthalene SOA in SLF.[48] They attributed the increase in ROS yields to redox-reaction cycles involving oxidizing components in naphthalene SOA and antioxidants in SLF.[48] Further investigations are needed to explore the thorough mechanisms of HULIS redox potential changes and the detailed chemical pathways. In fact, numerous studies reported that redox reactions between quinones and lung fluid antioxidants lead to ROS generation.[12,66] These redox cycles involve electron transfer from antioxidants to quinones, leading to the formation of semiquinones, followed by the regeneration of quinones through reactions with $O_2$ to form $O_2^{\cdot-}$. $O_2^{\cdot-}$ can further convert into $H_2O_2$, which is the most abundant and central ROS to radical reaction cycles and cause for oxidative stress in the respiratory tract. However, our study demonstrated that the redox-active constituents can be depleted or deactivated in the redox reactions, likely due to ROS reactions. In fact, $HO_2\cdot$/$O_2^{\cdot-}$ exhibits relatively high reaction rate constants with quinone and phenolic moieties.[67,68] In addition, a significant yield of $OH^{\cdot}$ was measured during the oxidation of reduced humic acids by oxygen in the absence of light.[69] $OH^{\cdot}$ can attack phenols and quinones, resulting in ring opening and mineralization of these redox-active compounds.[4,70] Our results reveal that atmospheric transformations determine the kinetics of the intrinsic redox reactions involving oxidizing and antioxidant compositions of HULIS in a neutral lung fluid environment.

## 4. Conclusions and atmospheric implications

This study represents the first investigation into the changes of antioxidant capacity (AOC) and oxidative potential (OP) of HULIS during nighttime atmospheric aging and subsequent aqueous evolution in human lung fluid mimics. The results indicate that fresh HULIS released from wood smoldering burning contain a high fraction of phenolic components, which contribute significantly to the AOC of HULIS. However, nighttime atmospheric reactions of HULIS with $O_3$ or $NO_3^{\cdot}$ lead to a reduction in both AOC and OP, indicating the decomposition or deactivation of redox-active compounds in HULIS aerosols. The rate constants involved in depleting HULIS redox-active moieties vary depending on the reaction pathways, resulting in different atmospheric lifetimes of antioxidant moieties and oxidizing components of HULIS. Furthermore, ambient humidity plays a significant role in facilitating the uptake of $O_3$ by HULIS and accelerating the associated reactions, promoting substantial oxidation, and causing fragmentation of HULIS aerosols. Consequently, the involvement of RH contributes to lower HULIS redox potential following $O_3$ oxidation, resulting in shorter lifetimes of HULIS redox-active components and limiting their potential health impacts.

Atmospheric aging modifies the cytotoxic effects of HULIS on lung epithelial cells (A549) in a similar pattern to the changes in HULIS OP, supporting the use of $OP^{DTT}$ as a promising indicator for evaluating HULIS toxicity. The study also reveals strong correlations between OP, A549 cell death, cellular ROS generation, and lipid peroxidation in response to HULIS exposure, highlighting oxidative stress as the primary toxic mechanism of HULIS.

Furthermore, when HULIS aerosol are deposited into lung fluid, rapid intrinsic reactions occur, as evidenced by the exponential decrease in HULIS AOC and OP, accompanied by the generation of $H_2O_{2eq}$ in a neutral environment (*i.e.*, PBS solution). The interactions between quinoid components and phenolic antioxidants in HULIS lead to $H_2O_{2eq}$ generation and also decompose or deactivate the redox-active components. Moreover, the pathways and extent of atmospheric aging determine the intrinsic evolution of HULIS in the lung fluid. Specifically, nighttime aging reduces the redox-active compounds of HULIS aerosols, resulting in relatively weaker aqueous reactions, a slower decline in HULIS redox potential, and lower $H_2O_{2eq}$ yield under neutral lung fluid conditions. The final $H_2O_{2eq}$ yields of fresh and atmospherically aged HULIS in a neutral environment are doubled in the presence of additional antioxidants (*i.e.*, SLF), confirming the importance of antioxidants in redox cycling and in $H_2O_{2eq}$ generation, and also suggests that the interactions among HULIS, biological antioxidants, and the lung system are the dominate source of $H_2O_{2eq}$, rather than the intrinsic chemical reactions within HULIS. These findings support recent studies reporting that endogenous ROS generation exceeds exogenous sources in the respiratory system upon inhalation of organic aerosols.[71–73] Furthermore, the trivial decrease in HULIS redox potential resulting from intrinsic chemistry implies that other channels, such as interaction with the respiratory system, are of greater importance in clearing organic toxicants.

A recent opinion review has emphasized the necessity of a better understanding of multiphase chemistry triggered by respirable particles at the lung–air interface to address the health impacts of harmful particles.[74] We acknowledge the limitations of the current investigation on HULIS aerosol, including the lack of speciation and quantification of the target organic toxicant/redox-active compounds, as well as the exact reaction pathways following atmospheric transformation and aging in the lung fluid environment. The simplified lung fluid mimics of PBS and SLF cannot fully replicate the conditions in the respiratory system, which is a complicated chemical environment incorporating antioxidants, surfactants, and proteins and involving biological interactions with the alveoli epithelial cells. The causal relationship between the dynamic evolution of aerosol in lung fluid and their final cytotoxic effects also requires further elucidation. Moreover, atmospheric organic aerosols from diverse sources are more intricate than the HULIS, and there are more complex transformation processes

beyond the simple nighttime simulations *via* $O_3$ or $NO_3^{\bullet}$, such as continuous diel agings of aerosols during their long-term transport. The three scenarios explored can hardly tell the lifetime behaviors of organic aerosols in the air, not even in the respiratory system. Overall, the primary objective of this study was to offer an initial holistic view of the dynamic redox potential and toxic evolution of typical biomass-burning organic pollutants delivered from the atmosphere to the respiratory system. However, the identified limitations underscore the necessity for further and wider research in this field.

## Conflicts of interest

There are no conflicts to declare.

## Author contributions

C. L. and Y. R. designed the study; C. L. conducted experiments in HULIS preparation, aging, characterization, and sampling; D. C, A. L., and C. D. analyzed the molecular composition; M. L. tested the cytotoxicity of HULIS; C. L. drafted the script with contributions from all co-authors.

## Acknowledgements

The study was partially supported by the Israel Science Foundation (ISF, grant #3205/19) and by Horizon Europe Framework Program (EASVOLEE, No. 101095457). YR, D. C and AL acknowledge additional support from the US National Science Foundation (Grant No. AGS-2039985/US-Israel Binational Science Foundation, BSF Grant No. 2020656).

## References

1 E. R. Graber and Y. Rudich, Atmospheric HULIS: How humic-like are they? A comprehensive and critical review, *Atmos. Chem. Phys.*, 2006, **25**, 729–753.
2 S. Huang, Y. Luo, X. Wang, T. Zhang, Y. Lei, Y. Zeng, J. Sun, H. Che, H. Xu and J. Cao, Optical properties, chemical functional group, and oxidative activity of different polarity levels of water-soluble organic matter in PM2.5 from biomass and coal combustion in rural areas in Northwest China, *Atmos. Environ.*, 2022, 119179.
3 M. W. Jones, J. T. Abatzoglou, S. Veraverbeke, N. Andela, G. Lasslop, M. Forkel, A. J. Smith, C. Burton, R. A. Betts and G. R. van der Werf, Global and regional trends and drivers of fire under climate change, *Rev. Geophys.*, 2022, **60**, e2020RG000726.
4 C. Li, Z. Fang, H. Czech, E. Schneider, C. P. Rüger, M. Pardo, R. Zimmermann, J. Chen, A. Laskin and Y. Rudich, pH modifies the oxidative potential and peroxide content of biomass burning HULIS under dark aging, *Sci. Total Environ.*, 2022, 155365.
5 X. Xu, X. Lu, X. Li, Y. Liu, X. Wang, H. Chen, J. Chen, X. Yang, T.-M. Fu and Q. Zhao, ROS-generation potential of Humic-like substances (HULIS) in ambient PM2. 5 in urban Shanghai: Association with HULIS concentration and light absorbance, *Chemosphere*, 2020, **256**, 127050.
6 Y. Zhang, J. J. Schauer, M. M. Shafer, M. P. Hannigan and S. J. Dutton, Source apportionment of *in vitro* reactive oxygen species bioassay activity from atmospheric particulate matter, *Environ. Sci. Technol.*, 2008, **42**, 7502–7509.
7 J. L. Mauderly and J. C. Chow, Health effects of organic aerosols, *Inhalation Toxicol.*, 2008, **20**, 257–288.
8 A. Laskin, J. Laskin and S. A. Nizkorodov, Chemistry of atmospheric brown carbon, *Chem. Rev.*, 2015, **115**, 4335–4382.
9 C. Li, Q. He, Z. Fang, S. S. Brown, A. Laskin, S. R. Cohen and Y. Rudich, Laboratory Insights into the Diel Cycle of Optical and Chemical Transformations of Biomass Burning Brown Carbon Aerosols, *Environ. Sci. Technol.*, 2020, **54**, 11827–11837.
10 C. Li, Q. He, J. Schade, J. Passig, R. Zimmermann, D. Meidan, A. Laskin and Y. Rudich, Dynamic changes in optical and chemical properties of tar ball aerosols by atmospheric photochemical aging, *Atmos. Chem. Phys.*, 2019, **19**, 139–163.
11 P. J. Ziemann and R. Atkinson, Kinetics, products, and mechanisms of secondary organic aerosol formation, *Chem. Soc. Rev.*, 2012, **41**, 6582.
12 T. Fang, P. S. Lakey, R. J. Weber and M. Shiraiwa, Oxidative potential of particulate matter and generation of reactive oxygen species in epithelial lining fluid, *Environ. Sci. Technol.*, 2019, **53**, 12784–12792.
13 T. Ihantola, M.-R. Hirvonen, M. Ihalainen, H. Hakkarainen, O. Sippula, J. Tissari, S. Bauer, S. Di Bucchianico, N. Rastak and A. Hartikainen, Genotoxic and inflammatory effects of spruce and brown coal briquettes combustion aerosols on lung cells at the air-liquid interface, *Sci. Total Environ.*, 2022, **806**, 150489.
14 S. Offer, E. Hartner, S. Di Bucchianico, C. Bisig, S. Bauer, J. Pantzke, E. J. Zimmermann, X. Cao, S. Binder and E. Kuhn, Effect of atmospheric aging on soot particle toxicity in lung cell models at the air-liquid interface: differential toxicological impacts of biogenic and anthropogenic secondary organic aerosols (SOAs), *Environ. Health Perspect.*, 2022, **130**, 027003.
15 M. Pardo, C. Li, Z. Fang, S. Levin-Zaidman, N. Dezorella, H. Czech, P. Martens, U. Käfer, T. Gröger and C. P. Rüger, Toxicity of Water-and Organic-Soluble Wood Tar Fractions from Biomass Burning in Lung Epithelial Cells, *Chem. Res. Toxicol.*, 2021, **34**, 1588–1603.
16 M. Pardo, C. Li, Q. He, S. Levin-Zaidman, M. Tsoory, Q. Yu, X. Wang and Y. Rudich, Mechanisms of lung toxicity induced by biomass burning aerosols, *Part. Fibre Toxicol.*, 2020, **17**, 1–15.
17 K. R. Daellenbach, G. Uzu, J. Jiang, L.-E. Cassagnes, Z. Leni, A. Vlachou, G. Stefenelli, F. Canonaco, S. Weber, A. Segers, J. J. P. Kuenen, M. Schaap, O. Favez, A. Albinet, S. Aksoyoglu, J. Dommen, U. Baltensperger, M. Geiser, I. El Haddad, J.-L. Jaffrezo and A. S. H. Prévôt, Sources of particulate-matter air pollution and its oxidative potential in Europe, *Nature*, 2020, **587**, 414–419.

18 C. Molina, R. Toro A, C. A. Manzano, S. Canepari, L. Massimi and M. A. Leiva-Guzmán, Airborne aerosols and human health: Leapfrogging from mass concentration to oxidative potential, *Atmosphere*, 2020, **11**, 917.

19 P. Lin and J. Z. Yu, Generation of Reactive Oxygen Species Mediated by Humic-like Substances in Atmospheric Aerosols, *Environ. Sci. Technol.*, 2011, **45**, 10362–10368.

20 Y. Ma, Y. Cheng, X. Qiu, G. Cao, Y. Fang, J. Wang, T. Zhu, J. Yu and D. Hu, Sources and oxidative potential of water-soluble humic-like substances (HULIS WS) in fine particulate matter ($PM_{2.5}$) in Beijing, *Atmos. Chem. Phys.*, 2018, **18**, 5607–5617.

21 O. I. Klein, N. A. Kulikova, I. S. Filimonov, O. V. Koroleva and A. I. Konstantinov, Long-term kinetics study and quantitative characterization of the antioxidant capacities of humic and humic-like substances, *J. Soils Sediments*, 2018, **18**, 1355–1364.

22 M. Aeschbacher, C. Graf, R. P. Schwarzenbach and M. Sander, Antioxidant properties of humic substances, *Environ. Sci. Technol.*, 2012, **46**, 4916–4925.

23 L. Bondareva and N. Kudryasheva, Direct and indirect detoxification effects of humic substances, *Agronomy*, 2021, **11**, 198.

24 P. H. Chowdhury, Q. He, R. Carmieli, C. Li, Y. Rudich and M. Pardo, Connecting the Oxidative Potential of Secondary Organic Aerosols with Reactive Oxygen Species in Exposed Lung Cells, *Environ. Sci. Technol.*, 2019, **53**, 13949–13958.

25 C. Li, M. V. Misovich, M. Pardo, Z. Fang, A. Laskin, J. Chen and Y. Rudich, Secondary organic aerosol formation from atmospheric reactions of anisole and associated health effects, *Chemosphere*, 2022, **308**, 136421.

26 M. Pardo, S. Offer, E. Hartner, S. Di Bucchianico, C. Bisig, S. Bauer, J. Pantzke, E. J. Zimmermann, X. Cao and S. Binder, Exposure to naphthalene and β-pinene-derived secondary organic aerosol induced divergent changes in transcript levels of BEAS-2B cells, *Environ. Int.*, 2022, **166**, 107366.

27 J. Wei, T. Fang and M. Shiraiwa, Effects of Acidity on Reactive Oxygen Species Formation from Secondary Organic Aerosols, *ACS Environ. Au*, 2022, **2**, 336–345.

28 J. Wei, T. Fang, C. Wong, P. S. Lakey, S. A. Nizkorodov and M. Shiraiwa, Superoxide Formation from Aqueous Reactions of Biogenic Secondary Organic Aerosols, *Environ. Sci. Technol.*, 2020, **55**, 260–270.

29 J. P. Wong, M. Tsagkaraki, I. Tsiodra, N. Mihalopoulos, K. Violaki, M. Kanakidou, J. Sciare, A. Nenes and R. J. Weber, Effects of atmospheric processing on the oxidative potential of biomass burning organic aerosols, *Environ. Sci. Technol.*, 2019, **53**, 6747–6756.

30 C. A. Weitekamp, T. Stevens, M. J. Stewart, P. Bhave and M. I. Gilmour, Health effects from freshly emitted *versus* oxidatively or photochemically aged air pollutants, *Sci. Total Environ.*, 2020, **704**, 135772.

31 C. M. Boyd, T. Nah, L. Xu, T. Berkemeier and N. L. Ng, Secondary organic aerosol (SOA) from nitrate radical oxidation of monoterpenes: effects of temperature, dilution, and humidity on aerosol formation, mixing, and evaporation, *Environ. Sci. Technol.*, 2017, **51**, 7831–7841.

32 P. J. Gallimore, P. Achakulwisut, F. D. Pope, J. F. Davies, D. R. Spring and M. Kalberer, Importance of relative humidity in the oxidative ageing of organic aerosols: case study of the ozonolysis of maleic acid aerosol, *Atmos. Chem. Phys.*, 2011, **11**, 12181–12195.

33 J.-H. Huang, F. Zhang, Y. P. Shi, J. R. Cai, Y. H. Chuang, W. P. Hu, Y. Y. Lee and C. C. Wang, Water Plays Multifunctional Roles in the Intervening Formation of Secondary Organic Aerosols in Ozonolysis of Limonene: A Valence Photoelectron Spectroscopy and Density Functional Theory Study, *J. Phys. Chem. Lett.*, 2023, **14**, 3765–3776.

34 S. S. Petters, S. M. Kreidenweis, A. P. Grieshop, P. J. Ziemann and M. D. Petters, Temperature-and humidity-dependent phase states of secondary organic aerosols, *Geophys. Res. Lett.*, 2019, **46**, 1005–1013.

35 J. H. Slade and D. A. Knopf, Multiphase OH oxidation kinetics of organic aerosol: The role of particle phase state and relative humidity, *Geophys. Res. Lett.*, 2014, **41**, 5297–5306.

36 K. Shimada, M. Nohchi, X. Yang, T. Sugiyama, K. Miura, A. Takami, K. Sato, X. Chen, S. Kato and Y. Kajii, Degradation of PAHs during long range transport based on simultaneous measurements at Tuoji Island, China, and at Fukue Island and Cape Hedo, Japan, *Environ. Pollut.*, 2020, **260**, 113906.

37 M. Shiraiwa, Y. Li, A. P. Tsimpidi, V. A. Karydis, T. Berkemeier, S. N. Pandis, J. Lelieveld, T. Koop and U. Pöschl, Global distribution of particle phase state in atmospheric secondary organic aerosols, *Nat. Commun.*, 2017, **8**, 15002.

38 W. Y. Tuet, Y. Chen, S. Fok, J. A. Champion and N. L. Ng, Inflammatory responses to secondary organic aerosols (SOA) generated from biogenic and anthropogenic precursors, *Atmos. Chem. Phys.*, 2017, **17**, 11423–11440.

39 Z. C. Decker, K. J. Zarzana, M. Coggon, K.-E. Min, I. Pollack, T. B. Ryerson, J. Peischl, P. Edwards, W. P. Dubé and M. Z. Markovic, Nighttime chemical transformation in biomass burning plumes: a box model analysis initialized with aircraft observations, *Environ. Sci. Technol.*, 2019, **53**, 2529–2538.

40 A. Patel, R. Satish and N. Rastogi, Remarkably High Oxidative Potential of Atmospheric $PM_{2.5}$ Coming from a Large-Scale Paddy-Residue Burning over the Northwestern Indo-Gangetic Plain, *ACS Earth Space Chem.*, 2020, **7**, 504–510.

41 Q. He, S. Tomaz, C. Li, M. Zhu, D. Meidan, M. Riva, A. Laskin, S. S. Brown, C. George and X. Wang, Optical Properties of Secondary Organic Aerosol Produced by Nitrate Radical Oxidation of Biogenic Volatile Organic Compounds, *Environ. Sci. Technol.*, 2021, **55**, 2878–2889.

42 C. Li, Q. He, A. P. S. Hettiyadura, U. Käfer, G. Shmul, D. Meidan, R. Zimmermann, S. S. Brown, C. George and A. Laskin, Formation of secondary brown carbon in

biomass burning aerosol proxies through $NO_3$ radical reactions, *Environ. Sci. Technol.*, 2019, **54**, 1395–1405.

43 E. A. Bruns, I. El Haddad, A. Keller, F. Klein, N. K. Kumar, S. M. Pieber, J. C. Corbin, J. G. Slowik, W. H. Brune and U. Baltensperger, Inter-comparison of laboratory smog chamber and flow reactor systems on organic aerosol yield and composition, *Atmos. Meas. Tech.*, 2015, **8**, 2315–2332.

44 R. C. Chapleski, Y. Zhang, D. Troya and J. R. Morris, Heterogeneous chemistry and reaction dynamics of the atmospheric oxidants, $O_3$, $NO_3$, and OH, on organic surfaces, *Chem. Soc. Rev.*, 2016, **45**, 3731–3746.

45 P. Lin, L. T. Fleming, S. A. Nizkorodov, J. Laskin and A. Laskin, Comprehensive molecular characterization of atmospheric brown carbon by high resolution mass spectrometry with electrospray and atmospheric pressure photoionization, *Anal. Chem.*, 2018, **90**, 12493–12502.

46 Y. Zhang, K. Wang, H. Tong, R.-J. Huang and T. Hoffmann, The maximum carbonyl ratio (MCR) as a new index for the structural classification of secondary organic aerosol components, *Rapid Commun. Mass Spectrom.*, 2021, **35**, e9113.

47 P. Shahpoury, Z. W. Zhang, A. Filippi, S. Hildmann, S. Lelieveld, B. Mashtakov, B. R. Patel, A. Traub, D. Umbrio and M. Wietzoreck, Inter-comparison of oxidative potential metrics for airborne particles identifies differences between acellular chemical assays, *Atmos. Pollut. Res.*, 2022, **13**, 101596.

48 H. Tong, P. S. J. Lakey, A. M. Arangio, J. Socorro, F. Shen, K. Lucas, W. H. Brune, U. Pöschl and M. Shiraiwa, Reactive Oxygen Species Formed by Secondary Organic Aerosols in Water and Surrogate Lung Fluid, *Environ. Sci. Technol.*, 2018, 11642–11651.

49 M. Wang, S. Qiu, H. Yang, Y. Huang, L. Dai, B. Zhang and J. Zou, Spectrophotometric determination of hydrogen peroxide in water with peroxidase-catalyzed oxidation of potassium iodide and its applications to hydroxylamine-involved Fenton and Fenton-like systems, *Chemosphere*, 2021, **270**, 129448.

50 D. J. Dijck-Brouwer, F. A. Muskiet, R. H. Verheesen, G. Schaafsma, A. Schaafsma and J. M. Geurts, Thyroidal and Extrathyroidal Requirements for Iodine and Selenium: A Combined Evolutionary and (Patho) Physiological Approach, *Nutrients*, 2022, **14**, 3886.

51 M. Lin and J. Z. Yu, Dithiothreitol (DTT) concentration effect and its implications on the applicability of DTT assay to evaluate the oxidative potential of atmospheric aerosol samples, *Environ. Pollut.*, 2019, **251**, 938–944.

52 K. I. Berker, F. A. Ozdemir Olgun, D. Ozyurt, B. Demirata and R. Apak, Modified Folin–Ciocalteu antioxidant capacity assay for measuring lipophilic antioxidants, *J. Agric. Food Chem.*, 2013, **61**, 4783–4791.

53 S. Kupina, C. Fields, M. C. Roman and S. L. Brunelle, Determination of total phenolic content using the Folin-C assay: Single-laboratory validation, First action 2017.13, *J. AOAC Int.*, 2018, **101**, 1466–1472.

54 R. L. Prior, X. Wu and K. Schaich, Standardized methods for the determination of antioxidant capacity and phenolics in foods and dietary supplements, *J. Agric. Food Chem.*, 2005, **53**, 4290–4302.

55 M. G. Adam, P. T. Tran, N. Bolan and R. Balasubramanian, Biomass burning-derived airborne particulate matter in Southeast Asia: A critical review, *J. Hazard. Mater.*, 2021, **407**, 124760.

56 P. S. Lakey, T. Berkemeier, H. Tong, A. M. Arangio, K. Lucas, U. Pöschl and M. Shiraiwa, Chemical exposure-response relationship between air pollutants and reactive oxygen species in the human respiratory tract, *Sci. Rep.*, 2016, **6**, 1–6.

57 C. Baduel, M. E. Monge, D. Voisin, J.-L. Jaffrezo, C. George, I. E. Haddad, N. Marchand and B. D'Anna, Oxidation of atmospheric humic like substances by ozone: a kinetic and structural analysis approach, *Environ. Sci. Technol.*, 2011, **45**, 5238–5244.

58 C. Arata, N. Heine, N. Wang, P. K. Misztal, P. Wargocki, G. Beko, J. Williams, W. W. Nazaroff, K. R. Wilson and A. H. Goldstein, Heterogeneous ozonolysis of squalene: gas-phase products depend on water vapor concentration, *Environ. Sci. Technol.*, 2019, **53**, 14441–14448.

59 W. Liu, Y. Xu, W. Liu, Q. Liu, S. Yu, Y. Liu, X. Wang and S. Tao, Oxidative potential of ambient $PM_{2.5}$ in the coastal cities of the Bohai Sea, northern China: Seasonal variation and source apportionment, *Environ. Pollut.*, 2018, **236**, 514–528.

60 E. A. Pillar-Little, R. C. Camm and M. I. Guzman, Catechol oxidation by ozone and hydroxyl radicals at the air–water interface, *Environ. Sci. Technol.*, 2014, **48**, 14352–14360.

61 Z. Struyk and G. Sposito, Redox properties of standard humic acids, *Geoderma*, 2001, **102**, 329–346.

62 C. Liu, D. Chen and X. Chen, Atmospheric reactivity of methoxyphenols: a review, *Environ. Sci. Technol.*, 2022, **56**, 2897–2916.

63 J. Sun, Q. Mu, H. Kimura, V. Murugadoss, M. He, W. Du and C. Hou, Oxidative degradation of phenols and substituted phenols in the water and atmosphere: a review, *Adv. Compos. Hybrid Mater.*, 2022, **5**, 627–640.

64 B. Berlinger, D. G. Ellingsen, M. Náray, G. Záray and Y. Thomassen, A study of the bio-accessibility of welding fumes, *J. Environ. Monit.*, 2008, **10**, 1448–1453.

65 R. Munday, Autoxidation of naphthohydroquinones: effects of pH, naphthoquinones and superoxide dismutase, *Free Radical Res.*, 2000, **32**, 245–253.

66 J. G. Charrier, A. S. McFall, N. K. Richards-Henderson and C. Anastasio, Hydrogen peroxide formation in a surrogate lung fluid by transition metals and quinones present in particulate matter, *Environ. Sci. Technol.*, 2014, **48**, 7010–7017.

67 B. H. Bielski, D. E. Cabelli, R. L. Arudi and A. B. Ross, Reactivity of $HO_2/O_2^-$ radicals in aqueous solution, *J. Phys. Chem. Ref. Data*, 1985, **14**, 1041–1100.

68 X. Yang, F. L. Rosario-Ortiz, Y. Lei, Y. Pan, X. Lei and P. Westerhoff, Multiple roles of dissolved organic matter in advanced oxidation processes, *Environ. Sci. Technol.*, 2022, **56**, 11111–11131.

69 S. E. Page, M. Sander, W. A. Arnold and K. McNeill, Hydroxyl radical formation upon oxidation of reduced humic acids by oxygen in the dark, *Environ. Sci. Technol.*, 2012, **46**, 1590–1597.

70 M. S. Win, Z. Tian, H. Zhao, K. Xiao, J. Peng, Y. Shang, M. Wu, G. Xiu, S. Lu, S. Yonemochi and Q. Wang, Atmospheric HULIS and its ability to mediate the reactive oxygen species (ROS): A review, *J. Environ. Sci.*, 2018, **71**, 13–31.

71 E. Dovrou, S. Lelieveld, A. Mishra, U. Pöschl and T. Berkemeier, Influence of ambient and endogenous $H_2O_2$ on reactive oxygen species concentrations and OH radical production in the respiratory tract, *Environ. Sci.: Atmos.*, 2023, **3**, 1066–1074.

72 T. Fang, Y.-K. Huang, J. Wei, J. E. Monterrosa Mena, P. S. Lakey, M. T. Kleinman, M. A. Digman and M. Shiraiwa, Superoxide Release by Macrophages through NADPH Oxidase Activation Dominating Chemistry by Isoprene Secondary Organic Aerosols and Quinones to Cause Oxidative Damage on Membranes, *Environ. Sci. Technol.*, 2022, **56**, 17029–17038.

73 F. Liu, M. G. Saavedra, J. A. Champion, K. K. Griendling and N. L. Ng, Prominent contribution of hydrogen peroxide to intracellular reactive oxygen species generated upon exposure to naphthalene secondary organic aerosols, *Environ. Sci. Technol. Lett.*, 2020, **7**, 171–177.

74 J. Abbatt and A. Ravishankara, Opinion: Atmospheric Multiphase Chemistry: Past, Present, and Future, EGUsphere, 2023, preprint, pp. 1–33.